Progress In Electromagnetics Research, Vol. 116, 409–423, 2011

DISPERSION AND LOSSES IN SURFACE WAVEGUIDES CONTAINING DOUBLE NEGATIVE OR CHIRAL METAMATERIALS

J. R. Canto*, C. R. Paiva, and A. M. Barbosa

Instituto de Telecomunicações, Instituto Superior Técnico Av. Rovisco Pais 1, Lisboa 1049-001, Portugal

Abstract—In this article the influence of both dispersion and losses on waveguides with metamaterials is investigated. The analysis is focused on surface waveguides (planar interfaces and grounded slabs) containing either double-negative (DNG) or chiral metamaterials. The main goal is to show how the combined effect of material dispersion and losses with the structural dispersion affect the solutions of the modal equations. It is shown that this interplay is essential to obtain a correct modal analysis of these waveguides. Namely, the overall behavior can qualitatively change — so that it is not possible to state that the corresponding lossy case — even when a very small amount of losses is introduced — can be interpreted as a small perturbation of the lossless case.

1. INTRODUCTION

The response of a given medium to an applied electromagnetic field is not instantaneous. In fact, any material medium is made of electrons and nuclei that have a finite mass and hence the corresponding inertia should be accounted for in the constitutive relations. Furthermore, that response cannot vanish instantaneously when the applied field is removed: the medium takes a finite time to relax back to its initial quiescent state. These facts are elegantly conveyed, at the macroscopic level, through the Kramers-Kronig relations — a direct consequence of the principle of causality: the response cannot precede the stimulus [1]. In fact, the Kramers-Kronig dispersion relations state the intimate connection between dispersion (refraction) and losses (absorption).

In this article we will always denote by $\varepsilon = \varepsilon' + i\,\varepsilon'' \in \mathbb{C}$ and $\mu = \mu' + i\,\mu'' \in \mathbb{C}$ the relative permittivity and permeability,

Received 6 April 2011, Accepted 11 May 2011, Scheduled 16 May 2011

* Corresponding author: João R. Canto (joao.canto@lx.it.pt).

respectively. Accordingly, the index of refraction $n = n' + i\,n'' \in \mathbb{C}$ obeys the relation $n^2 = \varepsilon\mu$ so that, in particular,

$$2n'n'' = \varepsilon'\mu'' + \varepsilon''\mu'. \tag{1}$$

Due to entropy and as we are only considering passive media, then $\varepsilon'' > 0$, $\mu'' > 0$ and $n'' > 0$. A DNG (double-negative) medium corresponds to the situation where $\varepsilon' < 0$ and $\mu' < 0$; for a SNG (single negative) medium $\varepsilon'\mu' < 0$. On the other hand, a NIR (negative index of refraction) medium corresponds to $n' < 0$. Hence, for a DNG medium, the right hand side of (1) is negative whereas, for a NIR medium, the left hand side of (1) is negative. But then, according to (1), a DNG medium is necessarily a NIR medium; the converse, however, is not true [2].

It has been shown that the CW (continuous-wave) portions of a modulated pulse (i.e., excluding its leading and trailing edges) do obey the NIR features associated with a time-harmonic analysis [3].

In waveguides containing metamaterials with negative parameters it is expected that the material dispersion should be playing an important role. Although it may be reasonable to present dispersion diagrams for waveguides containing weakly dispersive DPS (double positive) media without taking into account the material dispersion, the same cannot be applicable to waveguides containing DNG media instead. Also, it should be investigated into what extent is it accurate to restrict the analysis to lossless dispersive models as in [4], i.e., disregarding losses. In fact, according to the Kramers-Kronig relations, if there is dispersion with negligible losses in some frequency region, there is absorption in some other region (including, eventually, the same region). Although a lossless dispersive model can be considered as a limit of a lossy and causal one, we should not forget something that is fundamental for guided wave propagation: the modal equation of a waveguide results from the application of the appropriate boundary conditions imposed by the structure that constitutes its geometry. Accordingly, the interplay between the dispersion model (that is used for the metamaterial with negative parameters) and the structural dispersion (that results from the boundary conditions) cannot be neglected. It is not at all obvious, actually, what may result from that interplay. Moreover, if losses are introduced in the constitutive relations, it is not possible to predict — without solving the whole problem — into what frequency region (or regions) those losses will have a significant impact on the dispersion diagram for the waveguide under analysis. These problems give rise to new aspects that should be properly examined — in spite of the fact that, for unbounded wave propagation in bulk media, they may not be so relevant after all. However, these new aspects have not received, as far as the authors are

aware, any specific attention from researchers until now [5–13], despite the fact that the topic of guided wave propagation in the presence of metamaterials has been the subject of a significant number of papers — see, e.g., [4] and references therein. Furthermore, for waveguides containing anisotropic or bianisotropic media with negative parameters (i.e., containing indefinite media) a similar reasoning applies. With this paper we intend to prompt a discussion on the relevance of these new features. However, only the simplest waveguides will be analyzed herein — namely, planar interfaces and grounded slabs. Also, only two types of media will be examined: DNG and chiral media. Nevertheless, we intend to show that even these simple examples are enough to provide a new assessment of the influence that small losses can bring to the overall dispersive behavior of modes in waveguides containing metamaterials.

2. MODAL ANALYSIS USING A CAUSAL DISPERSIVE MODEL

General chiral media can be characterized, in the frequency domain, by the constitutive relations [14]

$$\mathbf{D} = \varepsilon_0 \boldsymbol{\varepsilon} \cdot \mathbf{E} + i\sqrt{\varepsilon_0 \mu_0}\, \boldsymbol{\chi} \cdot \mathbf{H}, \tag{2}$$

$$\mathbf{B} = \mu_0 \boldsymbol{\mu} \cdot \mathbf{H} - i\sqrt{\varepsilon_0 \mu_0}\, \boldsymbol{\chi}^{\mathrm{T}} \cdot \mathbf{E}, \tag{3}$$

where $\boldsymbol{\chi} = \chi \mathbf{I} + \mathbf{N}$ ($\mathbf{I}$ is the unit dyadic), $\chi = tr\{\boldsymbol{\chi}\}/3$ and $\boldsymbol{\varepsilon}$, $\boldsymbol{\mu}$, $\mathbf{N}$ are symmetric dyadics. Guided electromagnetic wave propagation of the form $\exp[i(k_z z - \omega t)]$, where $k_z = \beta_z + i\alpha_z$ is the longitudinal wave number, will be analyzed. The effective propagation constant is $k_{eff} = k_z/k_0$, with $k_0 = \omega/c$, where $k_{eff} = n_{eff} + i\ell_{eff}$: n_{eff} is the effective refractive index; ℓ_{eff} is the effective leakage parameter. Two different geometries are studied: (i) an interface, where medium 1 ($x > 0$) is isotropic DPS (Figure 1(a)); (ii) a grounded dielectric slab waveguide, where medium 1 ($x > d$) is also isotropic DPS (Figure 1(b)).

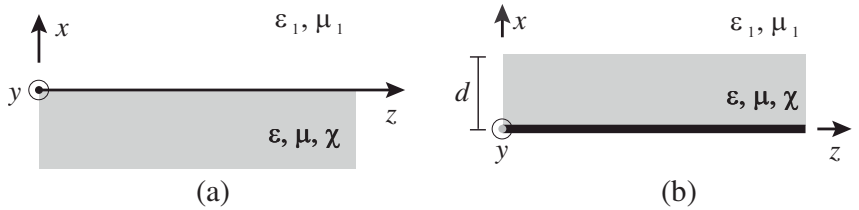

Figure 1. Structures under study: (a) Metamaterial-isotropic interface; (b) Metamaterial grounded slab.

Medium 2 is generally described by (2), (3). We have adopted the following Lorentz model to describe chiral media [15]

$$g_{\varepsilon}(\omega) = \varepsilon_{\infty} + \frac{(\varepsilon_s - \varepsilon_{\infty})\,\omega_{0e}^2}{\omega_{0e}^2 - \omega^2 - 2i\omega_{0e}^2\xi_e\omega}, \tag{4}$$

$$g_{\mu}(\omega) = \mu_{\infty} + \frac{(\mu_s - \mu_{\infty})\,\omega_{0m}^2}{\omega_{0m}^2 - \omega^2 - 2i\omega_{0m}^2\xi_m\omega}, \tag{5}$$

$$g_{\chi}(\omega) = \frac{\tau\omega_0^2\omega}{\omega_0^2 - \omega^2 - 2i\omega_0\xi\omega}. \tag{6}$$

In Table 1 we list the various types of chiral and achiral media that are going to be considered in this paper.

Table 1. Media analyzed in this paper.

Chiral	Isotropic	$\boldsymbol{\varepsilon} = g_{\varepsilon}(\omega)\mathbf{I}$
		$\boldsymbol{\mu} = g_{\mu}(\omega)\mathbf{I}$
		$\boldsymbol{\chi} = g_{\chi}(\omega)\mathbf{I}$
	Uniaxial	$\boldsymbol{\varepsilon} = \varepsilon_t(\hat{\mathbf{x}}\hat{\mathbf{x}} + \hat{\mathbf{y}}\hat{\mathbf{y}}) + \varepsilon_{zz}\hat{\mathbf{z}}\hat{\mathbf{z}},\ \varepsilon_{zz} = g_{\varepsilon}(\omega)$
		$\boldsymbol{\mu} = \mu_t(\hat{\mathbf{x}}\hat{\mathbf{x}} + \hat{\mathbf{y}}\hat{\mathbf{y}}) + \mu_{zz}\hat{\mathbf{z}}\hat{\mathbf{z}},\ \mu_{zz} = g_{\mu}(\omega)$
		$\boldsymbol{\chi} = \chi_{zz}\hat{\mathbf{z}}\hat{\mathbf{z}},\ \chi_{zz} = g_{\chi}(\omega)$
	Anisotropic	$\boldsymbol{\varepsilon} = \varepsilon_{xx}\hat{\mathbf{x}}\hat{\mathbf{x}} + \varepsilon_{yy}\hat{\mathbf{y}}\hat{\mathbf{y}} + \varepsilon_{zz}\hat{\mathbf{z}}\hat{\mathbf{z}}$
		$\boldsymbol{\mu} = \mu_{xx}\hat{\mathbf{x}}\hat{\mathbf{x}} + \mu_{yy}\hat{\mathbf{y}}\hat{\mathbf{y}} + \mu_{zz}\hat{\mathbf{z}}\hat{\mathbf{z}}$
		$\boldsymbol{\chi} = \chi_{xx}\hat{\mathbf{x}}\hat{\mathbf{x}} + \chi_{yy}\hat{\mathbf{y}}\hat{\mathbf{y}} + \chi_{zz}\hat{\mathbf{z}}\hat{\mathbf{z}}$
DNG		$\boldsymbol{\varepsilon} = g_{\varepsilon}(\omega)\mathbf{I},\ \Re\{g_{\varepsilon}(\omega)\} < 0$
		$\boldsymbol{\mu} = g_{\mu}(\omega)\mathbf{I},\ \Re\{g_{\mu}(\omega)\} < 0$
		$\boldsymbol{\chi} = \mathbf{0}$

For the specific case of uniaxial chiral media, a single orientation for the chiral inclusions — as shown in Figure 2 — is required.

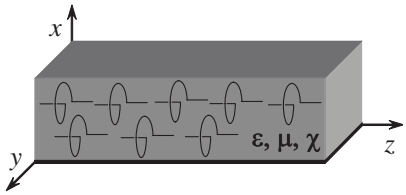

Figure 2. Helix orientation for the uniaxial chiral case.

We have assumed, in Table 1, that ε_t and μ_t do not depend on frequency. We have adopted, for our numerical calculations,

the following set of parameters: $\tau = 1.05 \times 10^{-11}$ s, $\xi_e = \xi_m = 2.65 \times 10^{-3}/\omega_0$, $\xi = 2.7 \times 10^{-3}$, $\omega_{0m} = \omega_0 = 3.662 \times 10^{10}$ rads^{-1}, $\omega_{0e} = 3.66 \times 10^{10}$ rads^{-1}. We have considered $\varepsilon_s = 1.95 + i\,7\delta_i$, $\mu_s = \mu_t$, $\varepsilon_\infty = 1.38 + i\,7\delta_i$, $\mu_\infty = 0.75 + i\,1.5\delta_i$, $\delta_i = 10^{-3}$ for the isotropic chiral case and $\varepsilon_s = 1.95 + i\,7.5\delta_u$, $\mu_s = \mu_t + i2.5\delta_u$, $\varepsilon_\infty = 1.38 + i\,7\delta_u$, $\mu_\infty = 0.75 + i\,2.5\delta_u$, $\delta_u = 10^{-2}$ for the uniaxial chiral case. The lossless case is obtained by setting $\xi_{e,m} = \delta_{i,u} = 0$. With these parameters, DNG/SNG/DPS regions are obtained in the 6–9 GHz frequency band, as shown in Figure 3.

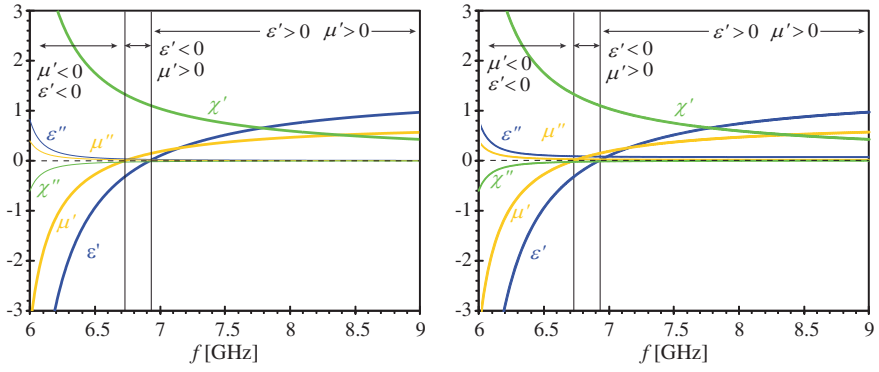

Figure 3. Dispersion curves for the real and imaginary parts of ε, μ and χ for medium 2: (a) Isotropic case; (b) Uniaxial case.

To distinguish among the several cases under study we have introduced the following simplified classification for the metamaterial: (i) DPS, if $\varepsilon', \mu' > 0$; (ii) SNG, if $\varepsilon' < 0$, $\mu' > 0$; (iii) DNG if $\varepsilon', \mu' < 0$ (Figure 3). Also, the results are obtained for left-handed chiral helices and, for the uniaxial case (Figure 3(b)), we have adopted $\varepsilon_t = 1.2 + i\,5\delta_{i,u}$ and $\mu_t = 1$. Furthermore, we have considered that the thickness of the grounded slabguides is $d = c/(4f_c)$ with $f_c = 6$ GHz since it allows to obtain representative modal results. Defining a loss coefficient such that

$$\rho = \max\left\{\varepsilon''/\varepsilon', \mu''/\mu', \chi''/\chi'\right\}, \tag{7}$$

it can be seen, from Figure 3, that $\rho \leq 10\%$ for frequency regions far from $\varepsilon' \approx 0$ and $\mu' \approx 0$. This cannot be considered as a small perturbation, but can however be considered as realistic (see for comparison the results in [17–19]). Also, [17] shows that, for chiral materials, at frequencies close to the resonance, losses can be much higher. Furthermore, [18] and [19] show that we can expect high levels

of losses when trying to obtain media with $\varepsilon' < 0$ and/or $\mu' < 0$, by adding metallic inclusions.

The modal equations for the chiral-isotropic interface and the grounded chiroslabguide can be written as

$$\eta_{11}\eta_{22} - \eta_{12}\eta_{21} = 0. \tag{8}$$

The derivation of the modal equations are detailed in Appendix A, where the expressions for η_{ij} $(i, j = 1, 2)$ are presented for the media considered in Table 1. At this point, one should note that, for an interface between two isotropic media, unrealistic results are obtained whenever losses are neglected: in this case, (8) reduces to

$$\alpha_a = \alpha_b = \alpha \rightarrow \left| \text{TE} \rightarrow \frac{\alpha_1}{\mu_1} + \frac{\alpha}{\mu} = 0; \quad \right| \text{TM} \rightarrow \frac{\alpha_1}{\varepsilon_1} + \frac{\alpha}{\varepsilon} = 0 \ . \tag{9}$$

According to this last equation a lossless DPS-DPS interface does not support any propagating modes. However, surface polaritons are possible at a DPS-DNG interface. Namely, for the TE case, we get

$$k_z = \pm \sqrt{\frac{\varepsilon\mu\mu_1^2 - \varepsilon_1\mu_1\mu^2}{\mu_1^2 - \mu^2}}. \tag{10}$$

But then, when losses are not taken into account, this last equation leads to the following unrealistic result:

$$\varepsilon\,\mu\,\mu_1^2 > \varepsilon_1\,\mu_1\,\mu^2 \rightarrow \lim_{\mu \rightarrow -\mu_1} k_z = \pm\infty. \tag{11}$$

This resonance is embedded in the modal equation, and is not a result of resonances of the constitutive parameters, it occurs at a frequency where the constitutive parameters have finite values as it can be seen in Figure 3. However, when losses are taken into account, one has $\mu_1^2 \neq \mu^2$ even for $\Re\{\mu_1\} = -\Re\{\mu\}$ and the resonance in (11) does not exist, see Figures 4(b) and 5(b) for the TE and TM modes, respectively.

In fact, for this simple case the resonance frequency has been analytically identified and it is shown that it does not exist in the presence of losses. For more complex cases, the solutions of the modal equations cannot be derived analytically, and only by solving the modal equations numerically can one find the frequencies where the resonances occur. To further illustrate the effect of taking losses into account, we present, in Figure 6, the effect of the chirality parameter on the effective propagation constant of a lossy isotropic chiral-air interface and compare it with the results obtained in [16] for the lossless case. Given that, our objective is to focus on the effect of losses, the results presented in Figure 6, do not take into account the dispersion model given by (4)–(6), since no dispersion model was used in [16]. A

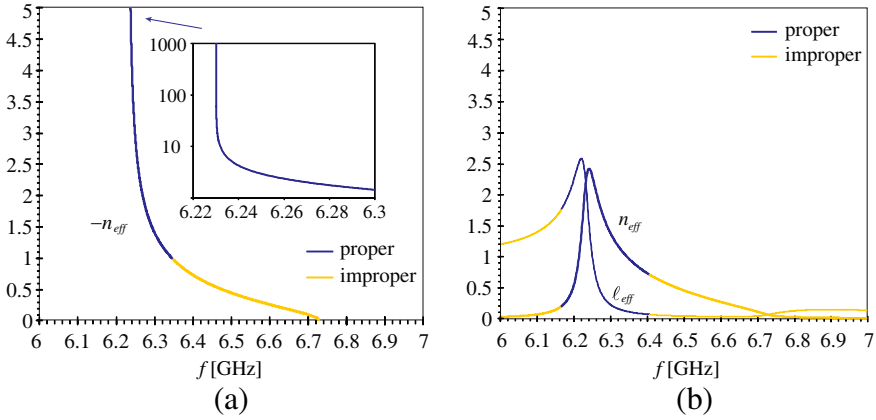

Figure 4. Dispersion diagram for the TE mode at an isotropic-air interface: (a) Lossless case; (b) Lossy case.

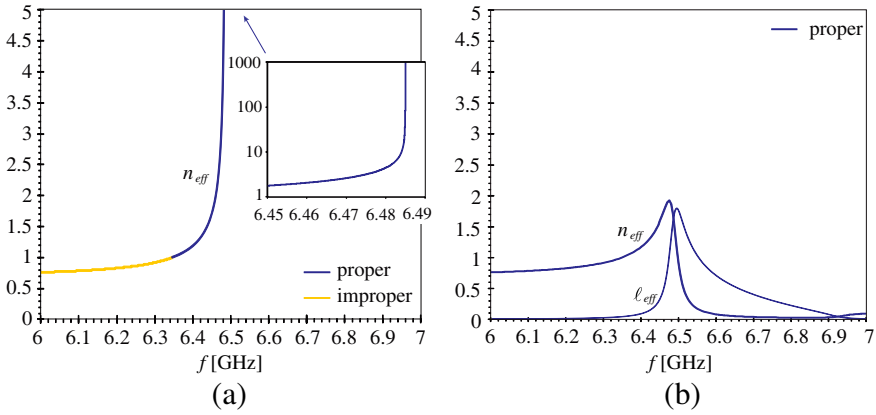

Figure 5. Dispersion diagram for the TM mode at an isotropic-air interface: (a) Lossless case; (b) Lossy case.

comparison between the results in Figure 6 and the results in [16], and the results in Figures 4 and 5 allow us to conclude that only accounting for losses physically meaningful results are obtained. Furthermore, the power flow along z, for the lossless DPS-DNG interface, is given by

$$P_z = \frac{1}{4}|A|^2 \left[\Re\left\{ \frac{k_z^*}{\mu_1^*} \right\} \frac{1}{\Re\{\alpha_1\}} + \Re\left\{ \frac{k_z^*}{\mu^*} \right\} \frac{1}{\Re\{\alpha\}} \right]. \qquad (12)$$

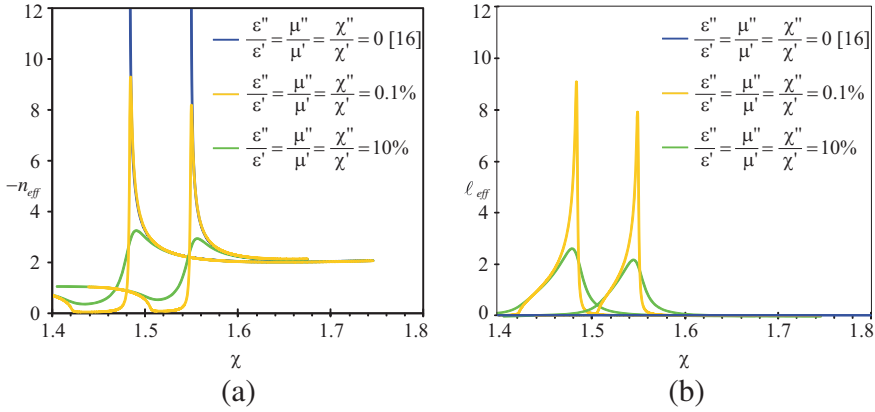

Figure 6. Effect of the chirality parameter χ on an isotropic chiral-air interface: (a) n_{eff}; (b) ℓ_{eff}. The results were obtained using the parameters as in [16].

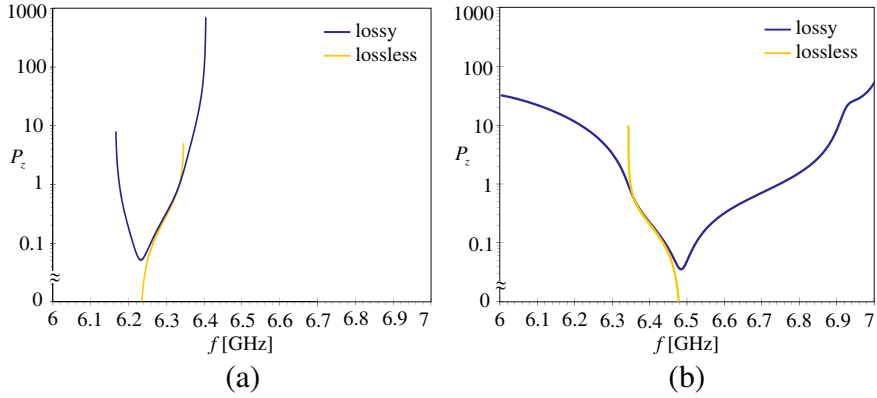

Figure 7. Power flow along the isotropic-air interface: (a) TE case; (b) TM case.

By taking the limit, we get

$$\left|\begin{array}{l}\lim\limits_{\mu\to-\mu_1}\alpha_1=k_z\\ \lim\limits_{\mu\to-\mu_1}\alpha=k_z\end{array}\right. \Rightarrow \lim_{\mu\to-\mu_1} P_z=\frac{1}{4}\frac{|A|^2}{\mu_1}\left[\frac{\Re\{k_z\}}{\Re\{\alpha_1\}}-\frac{\Re\{k_z\}}{\Re\{\alpha\}}\right]=0. \quad (13)$$

In fact, a mode having $k_z=\infty$ with zero power flow along z means that the structure would be able to slow down a wave until full stop. However, as shown in Figures 4 to 7, this behaviour is not realistic as it corresponds to a resonance in the modal equation that arises, if and

only if, losses are not accounted for. It is then clear that, when losses are not taken into account, the aforementioned results — resonances in k_z and null power flow — do arise as a consequence of the modal equation, and not of the dispersion model resonances (they occur far from the resonances of ε and μ). Note that, in Figure 7, for the frequency band under analysis, the power flow was obtained for proper surface modes only. Therefore, the endpoints of the lines correspond to the limits where the modal solutions transit to the improper sheet. As can be seen in the dispersion diagrams, surface polaritons were found to propagate at an isotropic-air interface. Furthermore, as derived in (11), the solutions of the modal equation present an unrealistic resonance when $\mu \to -\mu_1$, for TE modes ($\varepsilon \to -\varepsilon_1$ for TM modes), for the lossless case (Figures 4(a) and 5(a)). Moreover, as obtained in (13), the power flow along the interface heads toward zero for the same limits (Figure 7). Therefore, only accounting for losses physically acceptable results are obtained. Proper leaky modes (i.e., leaky modes that satisfy the radiation condition) can then be found to propagate at the interface (Figures 4(b) and 5(b)). Moreover, the frequency bands where proper or improper solutions occur are not correctly defined when losses are not taken into account. One should also note that, only when losses are taken into account, the correct sign of n_{eff} can be selected: in the DNG frequency band, the sign for the TE (TM) mode is negative (positive).

3. FURTHER NUMERICAL RESULTS AND DISCUSSION

In this section, further numerical results will be presented and discussed regarding chiral-air interfaces and chiral grounded slabguides. The Lorentz dispersion model, described in Section 2, is considered whenever losses are accounted for.

3.1. Chiral-Air Interfaces

In this section numerical results for chiral isotropic/uniaxial-air interfaces are presented. In Figure 8, we can see the dispersion diagram of an isotropic chiral-air interface, both for the lossless case, Figure 8(a), and for the lossy case, Figure 8(b). Once again, as for the isotropic-air interface (Figure 5), in the lossless case, a resonant behavior for k_z is observed, for finite values of ε, μ and χ. Only for the lossy case, a correct behavior for k_z is obtained: the resonance, of k_z, does not exist, and the frequency band, were the proper solution occurs, increases.

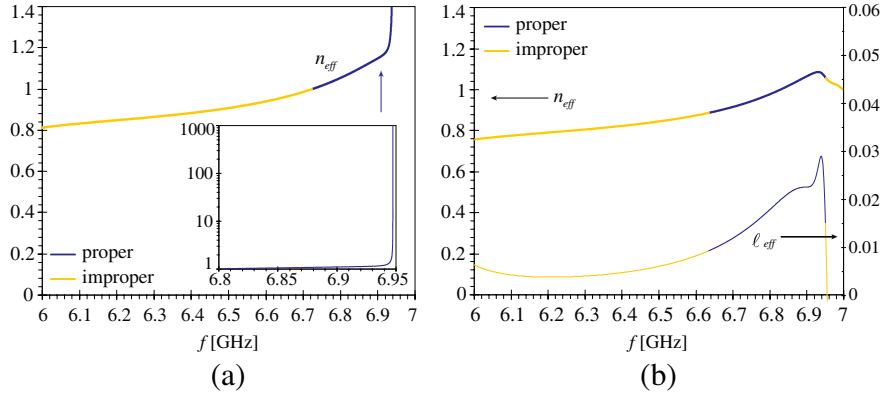

Figure 8. Dispersion diagram for an isotropic chiral-air interface: (a) Lossless case; (b) Lossy case.

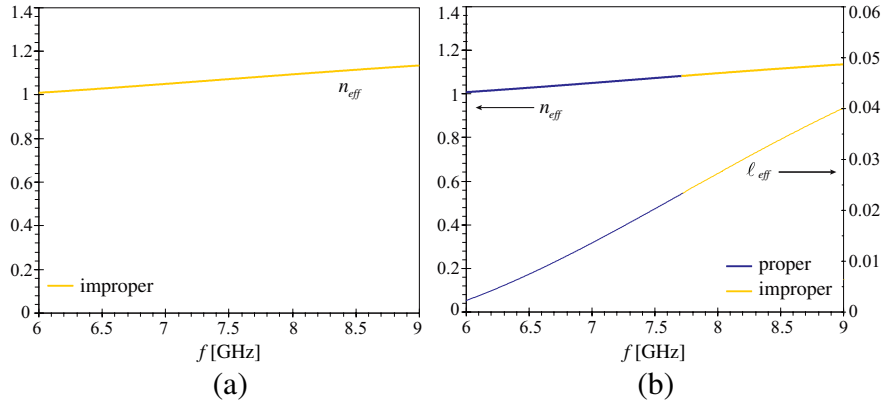

Figure 9. Dispersion diagram for a uniaxial chiral-air interface: (a) Lossless case; (b) Lossy case.

In Figure 9, the dispersion diagram of a uniaxial chiral-air interface is depicted, also for the lossless case and for the lossy case. These results reinforce our conclusion that the frequency bands where proper or improper solutions, of the modal equation, occur, can only be correctly found when losses are accounted for. In fact, only for the lossy case, can we observe a proper solution, in this frequency band.

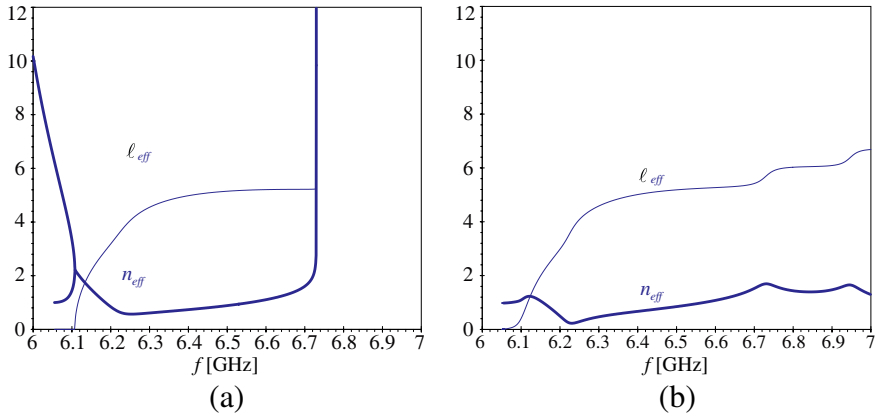

Figure 10. Dispersion diagram for a grounded isotropic chiroslabguide: (a) Lossless case; (b) Lossy case.

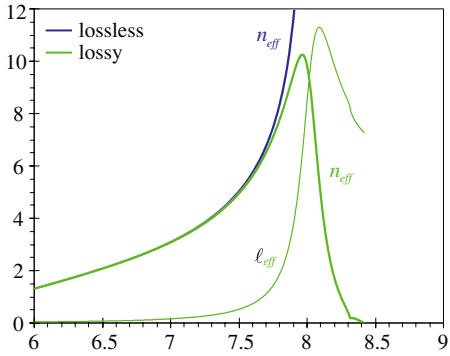

Figure 11. Dispersion diagram for a grounded uniaxial chiroslabguide.

3.2. Grounded Chiroslabguides

In this section numerical results for isotropic/uniaxial grounded chiroslabguides are presented. It is shown that both surface and proper leaky modes propagate in the lossless chiroslabguide (Figure 10(a)).

Collisions between surface modes, originating proper leaky modes are observed, as well as a resonant effect which causes $k_z \to \infty$. In the lossy case all modes are strictly leaky, and the collisions between modal solutions are no longer observed (Figure 10(b)). Moreover, the resonant behavior of k_z disappears, and the frequency band where proper solutions occur changes. Finally, a modal analysis of a uniaxial

grounded chiroslabguide is presented in Figure 11. Again, a resonant behavior in k_z is identified, which disappears in the lossy case. Note that, similarly to the isotropic chiroslabguide, the leakage coefficient ℓ_{eff} (in the lossy case) increases near the frequency where $k_z \to \infty$ (in the lossless case).

4. CONCLUDING REMARKS

We have shown that both dispersion and losses should be taken into account to correctly address a modal analysis in surface waveguides containing DNG or chiral metamaterials. It was shown that losses cannot be considered as a small perturbation of the lossless case. Indeed, only by taking losses into account, it is possible: (i) to avoid the ambiguity related to the choice of sign for the effective refractive index — even when the constitutive parameters of a given medium are all positive; (ii) to overcome the fact that modal equations can lead to solutions that exhibit a resonant behavior not directly related to the constitutive relations of the material; (iii) to obtain accurate results on the frequency bands where proper and improper modal solutions actually occur.

ACKNOWLEDGMENT

This work has been partially funded by the Foundation for Science and Technology, Portugal.

APPENDIX A. MODAL EQUATION

In this appendix, we derive the modal equation of the structures under study. We start by replacing the constitutive relations into the Maxwell equations thereby obtaining the following equation

$$\frac{\partial}{\partial x}\left[E_y \;\; H_z \;\; H_y \;\; E_z\right]^{\mathrm{T}} = i\,k_0 \begin{bmatrix} \mathbf{C}_{11} & \mathbf{C}_{12} \\ \mathbf{C}_{21} & \mathbf{C}_{22} \end{bmatrix} \left[E_y \;\; H_z \;\; H_y \;\; E_z\right]^{\mathrm{T}}, \quad \text{(A1)}$$

with

$$\mathbf{C}_{11} = \begin{bmatrix} 0 & Z_0\mu_{zz} \\ Y_0\varepsilon_{yy} - Y_0\varepsilon_{xx}\frac{k_z^2}{\Delta_x k_0^2} & 0 \end{bmatrix}, \quad \text{(A2)}$$

$$\mathbf{C}_{22} = \begin{bmatrix} 0 & -Y_0\varepsilon_{zz} \\ -Z_0\mu_{yy} + Z_0\mu_{xx}\frac{k_z^2}{\Delta_x k_0^2} & 0 \end{bmatrix}, \quad \text{(A3)}$$

$$\mathbf{C}_{12} = \mathbf{C}_{21} = \begin{bmatrix} 0 & -i\chi_{zz} \\ i\chi_{yy} + i\chi_{xx}\frac{k_z^2}{\Delta_x k_0^2} & 0 \end{bmatrix}, \quad \text{(A4)}$$

$Z_0 = 1/Y_0 = \sqrt{\mu_0/\varepsilon_0}$ and where $\Delta_x = \varepsilon_{xx}\mu_{xx} - \chi_{xx}^2$. Whenever $\mathbf{C}_{12} = \mathbf{C}_{21} \neq 0$, only hybrid modes are supported by the wave guiding structures. In fact it is still possible to rewrite (A1) as

$$\mathbf{\Phi} = [E_y \quad H_y]^T \rightarrow \frac{\partial^2 \mathbf{\Phi}}{\partial x^2} = -\mathbf{R} \cdot \mathbf{\Phi}, \tag{A5}$$

where $\mathbf{R}$ is a 2×2 coupling matrix given by

$$\begin{cases} R_{11} = (\mu_{zz}\varepsilon_{yy} + \chi_{zz}\chi_{yy})\, k_0^2 - (\mu_{zz}\varepsilon_{xx} - \chi_{zz}\chi_{xx})\, k_z^2/\Delta_x \\ R_{12} = iZ_0\,(\mu_{zz}\chi_{yy} + \chi_{zz}\mu_{yy})\, k_0^2 - iZ_0\,(\mu_{xx}\chi_{zz} - \mu_{zz}\chi_{xx})\, k_z^2/\Delta_x \\ R_{21} = -iY_0\,(\varepsilon_{zz}\chi_{yy} + \chi_{zz}\varepsilon_{yy})\, k_0^2 - iY_0\,(\varepsilon_{zz}\chi_{xx} - \chi_{zz}\varepsilon_{xx})\, k_z^2/\Delta_x \\ R_{22} = (\varepsilon_{zz}\mu_{yy} + \chi_{zz}\chi_{yy})\, k_0^2 - (\varepsilon_{zz}\mu_{xx} - \chi_{zz}\chi_{xx})\, k_z^2/\Delta_x \end{cases}. \tag{A6}$$

Furthermore, $\mathbf{R}$ can be diagonalized:

$$\mathbf{\Phi} = \mathbf{M} \cdot \mathbf{\Psi} \rightarrow \frac{\partial^2 \mathbf{\Psi}}{\partial\, x^2} = -\mathbf{\Lambda} \cdot \mathbf{\Psi}, \tag{A7}$$

where $\mathbf{M}$ is the modal matrix of $\mathbf{R}$. The transversal wave numbers, in medium 2, are then given by

$$h_s^2 = \frac{1}{2}\left(R_{11} + R_{22} \pm \sqrt{(R_{11} - R_{22})^2 + 4R_{12}R_{21}}\right) \tag{A8}$$

and hence

$$s = a, b \rightarrow \tau_s = \frac{h_s^2 - R_{11}}{R_{12}} \rightarrow \mathbf{M} = \begin{bmatrix} 1 & 1 \\ \tau_a & \tau_b \end{bmatrix}. \tag{A9}$$

Inside the chiral medium the field components are such that

$$\begin{cases} E_y = \Psi_a + \Psi_b \\ H_y = Y_0\ (\tau_a\, \Psi_a + \tau_b\, \Psi_b) \end{cases} \tag{A10}$$

where

$$\begin{cases} \text{chiral-isotropic interface} \rightarrow \Psi_s = A_s \exp(\alpha_s x) \\ \text{grounded chiroslabguide} \rightarrow \Psi_s = A_s \sin(h_s x) + B_s \cos(h_s x) \end{cases}, \tag{A11}$$

with $\alpha_s^2 = -\,h_s^2$. In the upper region the transversal attenuation constant is α_1, with $\alpha_1^2 = k_z^2 - \varepsilon_1\,\mu_1\,k_0^2$. After imposing the continuity of the tangential components of fields $\mathbf{E}$ and $\mathbf{H}$ at $z = 0$ (and $z = d$ for the slabguide), the modal equation is obtained:

$$\eta_{11}\eta_{22} - \eta_{12}\eta_{21} = 0, \tag{A12}$$

where:

$$\begin{cases} \eta_{11} = \varepsilon_1 \kappa_r^{(a)} \delta_\mu^{(a)} \rho_r^{(11)} + i\alpha_1 \left(\varepsilon_{zz}\mu_{zz} - \chi_{zz}^2\right) \sigma_r^{(11)} \\ \eta_{12} = \varepsilon_1 \left(\kappa_r^{(b)} \delta_\mu^{(b)} \rho_r^{(12)} + \kappa_r^{(a)} \delta_\mu^{(a)} \varsigma_r^{(12)}\right) + i\alpha_1 \left(\varepsilon_{zz}\mu_{zz} - \chi_{zz}^2\right) \sigma_r^{(12)} \\ \eta_{21} = \mu_1 \kappa_r^{(a)} \left(\delta_\varepsilon^{(a)} \rho_r^{(21)} + \delta_\varepsilon^{(b)} \varsigma_r^{(21)}\right) + i\alpha_1 \left(\varepsilon_{zz}\mu_{zz} - \chi_{zz}^2\right) \sigma_r^{(21)} \\ \eta_{22} = \mu_1 \left(\kappa_r^{(b)} \delta_\varepsilon^{(b)} \rho_r^{(22)} + \kappa_r^{(a)} \delta_\varepsilon^{(a)} \varsigma_r^{(22)}\right) + i\alpha_1 \left(\varepsilon_{zz}\mu_{zz} - \chi_{zz}^2\right) \sigma_r^{(22)} \end{cases}, \tag{A13}$$

Table A1. Coefficients for the modal equations.

$r =$ interface	$r =$ slab
$\kappa_r^{(a)} = \alpha_a$, $\kappa_r^{(b)} = \alpha_b$	$\kappa_r^{(a)} = h_a$, $\kappa_r^{(b)} = h_b$
$\rho_r^{(11)} = 1$, $\sigma_r^{(11)} = \tau_a$	$\rho_r^{(11)} = \cos(h_a d) - \cos(h_b d)$ $\sigma_r^{(11)} = \tau_a \sin(h_a d) - \frac{(i\mu_{zz}\tau_a - \chi_{zz})h_a}{(i\mu_{zz}\tau_b - \chi_{zz})h_b}\tau_b \sin(h_b d)$
$\rho_r^{(12)} = 1$, $\varsigma_r^{(12)} = 0$, $\sigma_r^{(12)} = \tau_b$	$\rho_r^{(12)} = \sin(h_b d)$, $\varsigma_r^{(12)} = -\sin(h_a d)$, $\sigma_r^{(12)} = \tau_a \cos(h_a d) - \tau_b \cos(h_b d)$
$\rho_r^{(21)} = 1$, $\varsigma_r^{(21)} = 0$ $\sigma_r^{(21)} = 1$	$\rho_r^{(21)} = -\cos(h_a d)$, $\varsigma_r^{(21)} = \frac{(i\mu_{zz}\tau_a - \chi_{zz})}{(i\mu_{zz}\tau_b - \chi_{zz})}\cos(h_b d)$ $\sigma_r^{(21)} = \frac{(i\mu_{zz}\tau_a - \chi_{zz})h_a}{(i\mu_{zz}\tau_b - \chi_{zz})h_b}\sin(h_b d) - \sin(h_a d)$
$\rho_r^{(22)} = 1, \varsigma_r^{(22)} = 0$, $\sigma_r^{(12)} = 1$	$\rho_r^{(22)} = -\sin(h_b d)$, $\varsigma_r^{(22)} = \sin(h_a d)$, $\sigma_r^{22} = \cos(h_b d) - \cos(h_a d)$

$\delta_\mu^{(s)} = i\tau_s\mu_{zz} - \chi_{zz}$ and $\delta_\varepsilon^{(s)} = i\varepsilon_{zz} + \tau_s\chi_{zz}$. The modal equations either for the interface or for the slab can then be readily derived from (A12) using the information from Tables 1 and A1.

REFERENCES

1. Kong, J. A., *Electromagnetic Wave Theory*, 595–597, EMW Publishing, Cambridge, MA, 2005.
2. McCall, M. W., A. Lakhtakia, and W. S. Weiglhofer, "The negative index of refraction demystified," *Eur. J. Phys.*, Vol. 23, 353–359, 2002.
3. Engheta, N. and R. W. Ziolkowski, Eds., *Metamaterials — Physics and Engineering Explorations*, IEEE Press/Wiley, Hoboken, NJ, 2006.
4. Baccarelli, P., et al., "Modal properties of layered metamaterials," *Theory and Phenomena of Metamaterials*, F. Capolino, Ed., CRC Press, Boca Raton, FL, 2009.
5. Dong, J., "Surface wave modes in chiral negative refraction grounded slab waveguides," *Progress In Electromagnetics Research*, Vol. 95, 153–166, 2009.
6. Naqvi, A., S. Ahmed, and Q. A. Naqvi, "Perfect electromagnetic conductor and fractional dual interface placed in a chiral nihility medium," *Journal of Electromagnetic Waves and Applications*, Vol. 24, No. 14–15, 1991–1999, 2010.
7. Xu, J., W. X. Wang, L. N. Yue, Y. B. Gong, and Y. Y. Wei, "Electromagnetic wave propagation in an elliptical chiroferrite waveguide," *Journal of Electromagnetic Waves and Applications*, Vol. 23, No. 14–15, 2021–2030, 2009.

8. Siakavara, K. and C. Damianidis, "Microwave filtering in waveguides loaded with artificial single or double negative materials realized with dielectric spherical particles in resonance," *Progress In Electromagnetics Research*, Vol. 95, 103–120, 2009.
9. Naqvi, Q. A., "Fractional dual solutions in grounded chiral nihility slab and their effect on outside fields," *Journal of Electromagnetic Waves and Applications*, Vol. 23, No. 5–6, 773–784, 2009.
10. Wu, Z., B. Q. Zeng, and S. Zhong, "A double-layer chiral metamaterial with negative index," *Journal of Electromagnetic Waves and Applications*, Vol. 24, No. 7, 983–992, 2010.
11. Topa, A. L., C. R. Paiva, and A. M. Barbosa, "Electromagnetic wave propagation in chiral H-guides," *Progress In Electromagnetics Research*, Vol. 103, 285–303, 2010.
12. Naqvi, A., A. Hussain, and Q. A. Naqvi, "Waves in fractional dual planar waveguides containing chiral nihility metamaterial," *Journal of Electromagnetic Waves and Applications*, Vol. 24, Nos. 11–12, 1575–1586, 2010.
13. Canto, J. R., C. R. Paiva, and A. M. Barbosa, "Modal analysis of bi-isotropic H-guides," *Progress In Electromagnetics Research*, Vol. 111, 1–24, 2011.
14. Serdyukov, A., I. Semchenko, S. Tretyakov, and A. Sihvola, *Electromagnetics of Bi-anisotropic Materials: Theory and Applications*, Gordon and Breach, Amsterdam, 2001.
15. Barba, I., A. Grande, A. C. L. Cabeceira, and J. Represa, "A multiresolution model of transient microwave signals in dispersive chiral media," *IEEE Trans. Antennas Propag.*, Vol. 54, 2808–2812, 2006.
16. Jin, Y., J. He, and S. He, "Surface polaritons and slow propagation related to chiral media supporting backward waves," *Phys. Lett. A*, Vol. 351, 354–358, 2006.
17. Brewitt-Taylor, C. R., P. G. Lederer, F. C. Smith, and S. Haq, "Measurement and prediction of helix-loaded chiral composites," *IEEE Trans. Antennas Propag.*, Vol. 47, 692–700, 1999.
18. Varadan, V. V. and A. R. Tellakula, "Effective properties of split-ring resonator metamaterials using measured scattering parameters: Effect of gap orientation," *Journal of Applied Physics*, Vol. 100, 034910, 2006.
19. Varadan, V., Z. Sheng, S. Penumarthy, and S. Puligalla, "Comparison of measurement and simulation of both amplitude and phase of reflected and transmitted fields in resonant omega media," *Microwave Opt. Technol. Lett.*, Vol. 48, 1549–1553, 2006.